Research Article Vol. 56, No. 35 / December 10 2017 / Applied Optics 9837

applied optics

Spectral characterization of a supercontinuum source based on nonlinear broadening in an aqueous K_2ZnCl_4 salt solution

Timothy S. Robinson,[1,*] Siddharth Patankar,[2] Emma Floyd,[3] Nicholas H. Stuart,[1] Nicholas Hopps,[3] and Roland A. Smith[1]

[1]Blackett Laboratory, Imperial College London, Prince Consort Road, London SW7 2AZ, UK
[2]Lawrence Livermore National Laboratory, P.O. Box 808, Livermore, California 94551, USA
[3]AWE plc, Aldermaston, Reading RG7 4PR, UK
*Corresponding author: timothy.robinson10@imperial.ac.uk

Received 7 September 2017; revised 18 October 2017; accepted 20 October 2017; posted 23 October 2017 (Doc. ID 306464); published 8 December 2017

We report on investigations concerning the shot-to-shot spectral stability properties of a supercontinuum source based on nonlinear processes such as self-phase modulation and optical wave-breaking in a highly concentrated K_2ZnCl_4 double salt solution. The use of a liquid medium offers both damage resistance and high third-order optical nonlinearity. Approximately 40 μJ pulses spanning a spectral range between 390 and 960 nm were produced with 3.8% RMS energy stability, using infrared input pulses of 500 ± 50 fs FWHM durations and 2.42 ± 0.04 mJ energies with an RMS stability of 2%. The spectral stability was quantified via acquiring single-shot spectra and studying shot-to-shot variation across a spectral range of 200–1100 nm, as well as by considering spectral correlations. The regional spectral correlation variations were indicative of nonlinear processes leading to sideband generation. Spectral stability and efficiency of energy transfer into the supercontinuum were found to weakly improve with increasing driver pulse energy, suggesting that the nonlinear broadening processes are more stable when driven more strongly, or that self-guiding effects in a filament help to stabilize the supercontinuum generation.

Published by The Optical Society under the terms of the Creative Commons Attribution 4.0 License. Further distribution of this work must maintain attribution to the author(s) and the published article's title, journal citation, and DOI.

OCIS codes: (320.6629) Supercontinuum generation; (140.0140) Lasers and laser optics; (190.0190) Nonlinear optics; (190.3270) Kerr effect; (190.4720) Optical nonlinearities of condensed matter; (140.7300) Visible lasers.
https://doi.org/10.1364/AO.56.009837

1. INTRODUCTION

A supercontinuum laser is an ultra-broadband source of light with high spatial coherence generated by nonlinear optical methods [1]. Because of their large bandwidths and coherence properties, white-light pulses are potentially compressible to extremely short transform-limited pulse durations [2–5], subject to appropriate management of spectral phase. Supercontinuum light sources may be used for a variety of purposes, including numerous biomedical applications [6] such as optical coherence tomography [7], fiber-optic communications [8], chemical sensing (spectroscopy) and microscopy [9], remote sensing and atmospheric analysis [10], and white-light interferometry. Typically, spectral broadening is achieved via propagating short or ultrashort pulses through highly nonlinear media, such as crystalline solids and other bulk materials [11], photonic crystal fibers (PCFs) [12–14], gas-filled [15,16] or liquid-filled hollow-core PCFs [17,18], or liquids [19–24]. Much of the reported work on supercontinuum sources and their stability focuses on fiber-based sources [25–30] or spectral broadening in solid bulk materials, such as YAG crystals [11,31]. Preceding works have used heterodyne detection techniques to study supercontinuum noise [32,33], and the dispersive time stretch technique, a powerful tool allowing real-time measurement, has been used to measure spectral fluctuations related to supercontinuum seeding [34] and spectra broadened by modulation instabilities [25,26], which typically contain fine structure that can vary considerably pulse-to-pulse. The spectral stability of supercontinua from liquid CS_2-filled fibers was studied by Chemnitz *et al.* [18], where molecular re-orientational effects contributing to the optical nonlinearity associated with elongated liquid molecules were found to

increase the pulse-to-pulse reproducibility of spectra compared to nonlinearity purely due to the electronic response.

A combination of nonlinear processes is often responsible for broadening; these might include self-phase modulation (SPM), optical wave breaking [35,36], modulation instabilities [25,37,38], four-wave mixing [39–41], soliton self-frequency shift effects [42–48], or stimulated Raman scattering. SPM arises as a consequence of the optical Kerr nonlinearity, where the refractive index of a material exhibits intensity dependence. The refractive index n of a material in this case is given by the well-known equation

$$n(\mathbf{r}, t) = n_0 + n_2 I(\mathbf{r}, t), \quad (1)$$

where $I(\mathbf{r}, t)$ describes the spatio-temporally varying laser pulse intensity profile, and n_2 is the material-dependent nonlinear refractive index. The spatially varying component of $n(\mathbf{r}, t)$ can lead to self-focusing, while the temporal variation results in SPM. For an initially unchirped pulse propagating through a normally dispersive medium, SPM leads to accumulation of chirp due to an instantaneous frequency shift across its temporal profile, and subsequent spectral broadening [49–51]. The combined effects of SPM and group velocity dispersion (GVD) were shown by Tomlinson *et al.* to lead to optical wave breaking, resulting in the formation of well-developed coherent spectral side lobes [35]; this occurs where the frequency-shifted light overruns the pulse tails, by either traveling faster than the non-shifted light at the leading edge or slower at the trailing edge, such that the interference between the shifted and non-shifted light generates new frequencies.

A pulsed supercontinuum source based on focusing ~500 fs infrared (IR) pulses (1054 nm center wavelength, 3.5 ± 0.2 nm FWHM bandwidth) into a concentrated K_2ZnCl_4 (aq) double-salt solution was developed and spectrally characterized for its stability at a range of input energies. The work reported in this paper describes a broadband spectral stability characterization of a supercontinuum generated in a liquid medium spanning the visible to near-IR spectral regions. Although other liquids or solvents, such as CS_2, have better transmission properties with high optical nonlinearities, there are some key advantages to using aqueous salt solutions. Compared to CS_2, which is teratogenic, highly toxic, volatile at room temperature, and flammable, the salt solutions pose far fewer handling risks beyond mild corrosiveness and unlikely accidental ingestion. As CS_2 evaporates at room temperature, it is unwise to photo-ionize a flammable liquid–gas mixture. Unlike salt solutions, nonlinear liquids such as CS_2 or toluene chemically degrade many common sealants, potentially leading to containment issues. In addition, we do not expect lifetime issues such as photochemical degradation to affect salt solutions; $ZnCl_2$ and KCl molecules in solution are already dissociated, unlike CS_2 or hydrocarbon molecules, which have been observed to dissociate following multiphoton ionization of inner-shell electrons by 200 fs IR pulses [52].

The linear optical absorption of aqueous salt solutions has been shown by Li *et al.* [53] to increase with salt concentration for wavelengths between 300 and 700 nm, although the change is less pronounced for near-IR wavelengths. The laser-induced bulk damage thresholds were measured for the K_2ZnCl_4 solution and pure water; these were found to be at pulse energies of 15 ± 4 μJ and 12 ± 3 μJ for the salt solution and pure water, respectively, suggesting that damage thresholds increase with salt concentration. A similar trend with salt solutions was found by Hammer *et al.* using 400 fs pulses [54]. As the light was focused into the center of a bulk liquid, the damage thresholds were not determined in terms of intensity or fluence, as the beam size at the breakdown point is not easily measurable, and hence are reported in terms of input energy. This short-pulse supercontinuum source was previously used for interferometry applications [55] and calibration of the absolute photon response of optical streak cameras in a fast-sweep mode for optical pyrometry diagnostics at the Orion laser facility [56], as this required high-brightness pulses on a picosecond timescale. Shot-to-shot stability is needed to ensure good reproducibility, essential for absolute streak camera calibration. Similarly, all multi-shot scanning applications benefit from spectrally and energetically stable pulses. Hence, the work reported in this paper is necessary to demonstrate the source's stability.

2. SPECTRAL STABILITY ANALYSIS

A. Optical Setup

The Cerberus laser at Imperial College London, a Nd:glass system using optical parametric chirped pulse amplification (OPCPA) capable of 10 Hz operation, was used to provide test pulses of up to 2.5 mJ with 500 ± 50 fs FWHM durations and 10.0 ± 0.5 mm $1/e^2$ beam widths. These were focused into cells containing the double-salt solution using a $f = 60$ mm plano-convex lens, in order to generate the supercontinuum within the focal volume under conditions of SPM and self-focusing, leading to filamentation. The focal spot size within the liquid was not possible to measure directly, and indeed varied with input energy due to self-focusing. The apparatus used to acquire spectra for characterizing the source's spectral stability is shown in Fig. 1.

Spectra were measured with a B&WTek BRC624E spectrometer, a modular grating/linear-CCD device with a manufacturer-quoted resolution of 1.8 nm within a spectral range of 190–1100 nm and built-in nonlinearity correction. All spectra were acquired as single-pulse spectra; this was achieved by electronically triggering the spectrometer and a physical shutter to ensure each acquisition corresponded to a single light pulse, with a trigger source synchronized to the laser system.

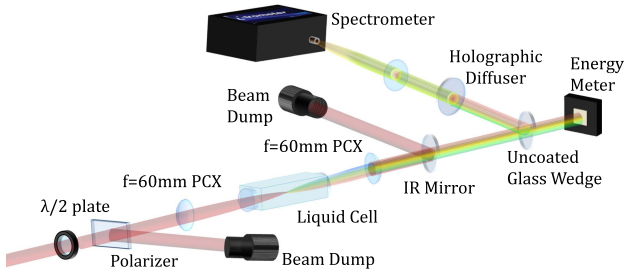


Fig. 1. Layout of the setup used to acquire spectra for analysis of the supercontinuum source's spectral stability. A holographic diffuser was used to spatially smooth the pulses in order to isolate the overall pulse-to-pulse spectral stability.

The acquisition time was set to 100 ms to minimize any detection of any stray light. A spectrum was then saved for each single acquisition. A $\lambda/2$ plate and polarizer were used to control the input pulse energies focused into the liquid cell, containing an aqueous K_2ZnCl_4 solution of concentration 652 ± 7 g/L. The liquid cell was 80 mm in length, and sealed at each end with an 8 mm thick N-BK7 window. An infrared mirror was used to direct the fundamental 1054 nm component into a beam dump. To prevent the spectrometer saturating, an uncoated glass wedge was used to pick off ~4% of the white light, which was focused into the spectrometer. As the pulses in our case were relatively energetic, a substantial signal could be recorded even with a single pulse coinciding with the acquisition time window. The transmitted component was directed onto a Gentec broadband surface-absorbing energy meter for simultaneous white-light energy monitoring capability. A holographic diffuser was used to spatially smooth the pulse's intensity profile prior to the spectrometer input to isolate the overall pulse-to-pulse spectral stability, in terms of generation of spectral content across the full beam, from any spatial inhomogeneity resulting in the spectrometer incompletely sampling the spectrum.

The energy content of the supercontinuum pulse (with the 1054 nm fundamental wavelength removed using an IR mirror) scales quadratically with the driver pulse energy within the range of energies considered (Fig. 2). This implies that the system efficiency of spectral broadening, defined here as the ratio of output supercontinuum energy (*after* removal of the fundamental wavelength) and input IR energy, weakly increases with input energy from $0.99 \pm 0.05\%$ to $1.57 \pm 0.06\%$.

The conversion efficiency is limited by the nonlinear medium's n_2 value and the interaction length over which the pulse is sufficiently intense for nonlinear effects to occur, which depends on factors such as the focal geometry and self-focusing in the liquid. For this reason, PCF supercontinuum sources typically exhibit higher conversion efficiencies due to their longer interaction lengths. However, the usable pump energy in PCF is relatively low due to the risk of damaging the fiber's internal structure, not an issue in our case. The supercontinuum pulse duration, broadened due to normal dispersion in the liquid, was measured to be ~5 ps using an optical streak camera with 1 ps time resolution. The source can be simply implemented and is resistant to damage from high light intensities breaking down the focal volume due to liquid media being "self-healing." Salt-solution-filled cells are low-cost relative to PCF, although a relatively powerful laser is required to drive the supercontinuum. The salt solution used for this study was chosen based on work by Jimbo *et al.*, who reported enhanced spectral broadening via SPM in concentrated salt solutions relative to water, due to increased nonlinearity by addition of metal cations [19].

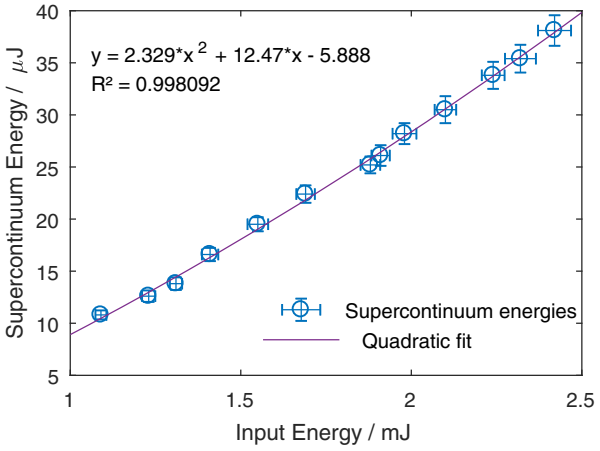


Fig. 2. Variation of the supercontinuum pulse energy with the input driver pulse energy, measured after removing the fundamental 1054 nm component using an IR mirror. Each data point is the mean value measured over 100 shots. A quadratic fit was found to match the data most closely. Error bars shown are the standard deviations of the mean input IR and supercontinuum energies.

B. Stability Results

A supercontinuum spectrum generated using 2.42 ± 0.04 mJ, 500 ± 50 fs, 1054 nm driver pulses and averaged over 50 shots is shown in Fig. 3. The standard deviation of the measured intensity counts at each wavelength point is shown as an error bar, with all 50 spectra displayed in gray to demonstrate the spatially integrated shot-to-shot variability. These show that the spectra remain very consistent shot-to-shot. From Fig. 3, it is clear that the stability is not constant across the full spectrum, hence it is important to characterize the stability over the widest possible wavelength range. An absorption profile for water [57] is overlaid on the spectrum in Fig. 3, and a predicted spectrum before and after propagation through 5 cm of water is shown in Fig. 4.

From these, it is apparent that the structure in the supercontinuum is partly modulated by light absorption in the solvent, as strong absorption features coincide with some troughs in the supercontinuum spectrum. As a linear process, the absorption modulations on the spectral shape are expected to be highly reproducible shot-to-shot. However, based on Fig. 4, the structure in the measured supercontinuum spectra can only partly be explained by absorption, and, hence, is

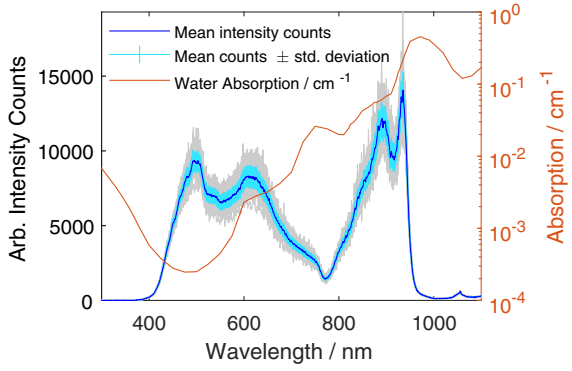


Fig. 3. Supercontinuum spectrum generated from the K_2ZnCl_4 (aq) solution using 1054 nm drive pulses of 2.42 ± 0.04 mJ and 500 ± 50 fs. The spectrum was spatially smoothed using a holographic diffuser, and averaged over 50 shots, with the ensemble standard deviation at each wavelength point shown as an error bar. All 50 spectra measured at this input energy are also shown in gray for comparison. The spectrum is overlaid with the water absorption profile [57].

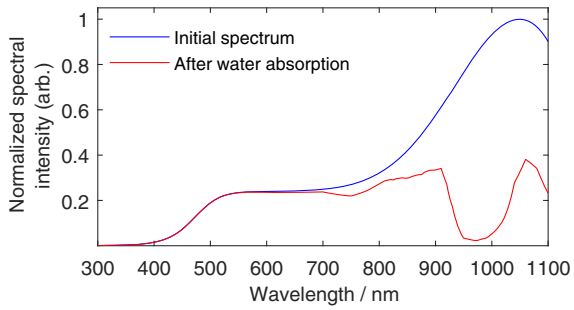


Fig. 4. Absorption curve for a broadened spectrum (with the driver centered on 1054 nm) before and after propagation through 5 cm of water, calculated using absorption data reported in [57]. Spectral intensities have been normalized to the peak of the initial spectrum.

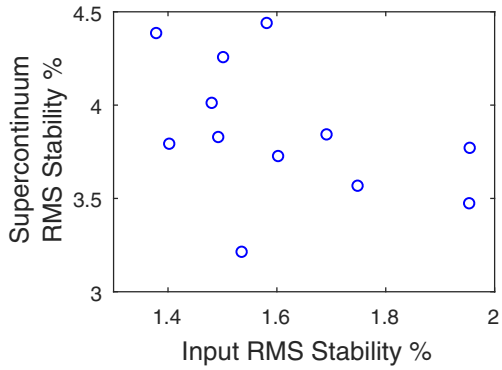


Fig. 5. Variation of the output RMS energy stability against input RMS; no clear correlation was observed. Each data point reflects the RMS stabilities about a particular mean energy value, where the mean energies range between 1.09 ± 0.02 and 2.42 ± 0.04 mJ.

possibly a signature of the underlying nonlinear processes, such as the occurrence of optical wave breaking following SPM and GVD. Spectral content above ~1000 nm is also largely removed by the high-reflectivity IR mirror used to remove the drive pulse; however, a residual component of this is nonetheless detected by the spectrometer. In addition, water has strong absorption bands above 1.2 μm, hence any generated longer wavelengths will be attenuated heavily within the liquid. For applications requiring broadband near- to mid-IR pulses generated in a liquid medium, the absorption on the spectral profile could be reduced by shortening the propagation path through the liquid, or alternatively using a liquid jet [22], at the expense of increased engineering complexity.

The spectrometer used for these measurements had a sampling (linear CCD pixel read-out) resolution (0.53 nm) higher than the manufacturer's quoted optical resolution (1.8 nm), and so there is additional uncertainty introduced to spectral measurements, on top of electrical and dark noise and shot-to-shot variation of the supercontinuum pulses, as a given pixel could detect photons with wavelengths outside of its 0.53 nm wide bin. Hence, the spectral intensity data was sorted into wavelength bins of 1.8 nm widths to reduce the effect of this wavelength-resolution pixel uncertainty when quantifying the spectral stability.

C. Scaling Properties with Input Energy

A key advantage of using a fluid for the nonlinear medium is its inherent resistance to permanent damage via photo-ionization, color center formation, or mechanical fracture. Ionic salt solutions are also already dissociated and therefore resistant to chemical degradation by bond breaking via irradiation over time. Hence, pulses with intensities exceeding the material breakdown threshold can be used to drive the supercontinuum, allowing larger broadband pulse energies to be obtained. Increasing the energy was found to be advantageous not only for supercontinuum generation efficiency, but also in terms of stability; if the nonlinear processes are driven further above the threshold intensities, small variations in input energy are expected to have less of an effect on output pulse properties than when operating very close to threshold. Alternatively, self-guiding effects in filaments [58,59] could help to stabilize the supercontinuum by maintaining a sufficiently small beamwidth in order to be above the threshold intensity for spectral broadening over longer interaction lengths. However, this requires a relatively smooth spatial pulse profile, as spatial intensity modulations are amplified by self-focusing, eventually resulting in multiple filaments or catastrophic beam breakup. The effect cannot be accounted for by considering only the input RMS energy stabilities; as shown in Fig. 5, where each data point was taken at a different mean input energy, there is no clear correlation between input and output RMS stabilities when measuring over a range of mean input energies, suggesting the output pulse stabilities must also be dependent on another variable.

The stability improvement with increasing drive energy was tested in the case of the K_2ZnCl_4 source by considering two metrics: the energy stability of the white-light measured using an energy meter and the spectral stability across the full spectrum over 50 shots. Spectral stability was quantified by considering the standard deviation (SD) of the measured intensity counts (as a percentage of the mean) at each wavelength value, or by considering standard deviations of spectral counts binned into variable wavelength bands. A reduction in the SD as percentage of the mean signifies an increase in the spectral stability.

The variation of global spectral stability σ_{glo} with input energy is shown in Fig. 6, where the quoted stability values are calculated by sorting spectral intensity data into 1.8 nm width wavelength bins, determining the SD (σ_{λ_i}) of intensity counts (I_{λ_i}) in each bin (λ_i), as a percentage of the mean value of intensity counts ($\overline{I}_{\lambda_i}$). We then calculate the mean of these SDs across the full spectrum to obtain an overall spectral stability value for each tested input laser energy. The spectral stability σ_{λ_i} of each wavelength bin as a percentage of $\overline{I}_{\lambda_i}$ is given by

$$\sigma_{\lambda_i} = \frac{100}{\overline{I}_{\lambda_i}} \sqrt{(\overline{I_{\lambda_i}^2}) - (\overline{I}_{\lambda_i})^2}, \tag{2}$$

where $\overline{X}$ denotes the mean of a variable X. For a given input energy, σ_{glo} is thus simply the mean of σ_{λ_i}, such that

$$\sigma_{\text{glo}} = \overline{\sigma}_{\lambda_i}. \tag{3}$$

1.8 nm bin widths were used to reduce the effect of the aforementioned pixel resolution uncertainty on the measured

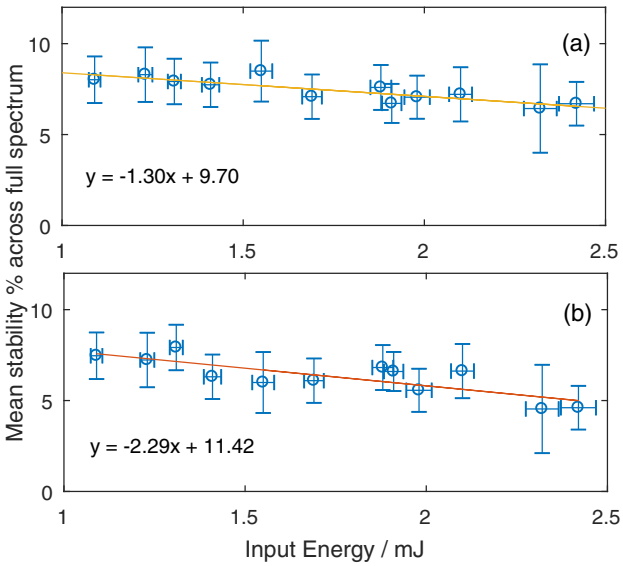


Fig. 6. Energy scaling of the global shot-to-shot spectral stability σ_{glo} in the cases of (a) no scaling to input RMS energy stability and (b) with the data scaled to the input RMS stability values for each energy. The metric for stability at each energy is quantified by sorting spectral intensity data into 1.8 nm bins, and calculating σ_{glo} using Eqs. (2) and (3). Uncertainties shown in the error bars reflect the standard deviations of the mean stability percentages for each input energy value.

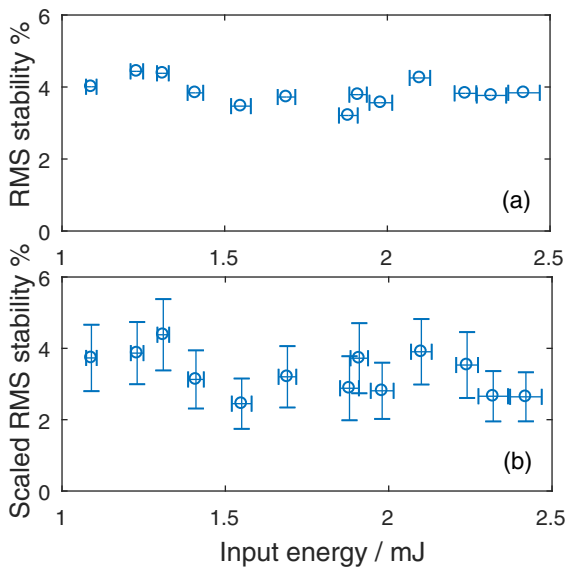


Fig. 7. Variation in the RMS energy stability in the supercontinuum pulse, measured using a broadband surface-absorbing Gentec energy meter. The data is presented (a) without and (b) with scaling to the input pulse RMS energy stabilities. The scaling factor applied to (b) was the ratio of the smallest percentage RMS stability of the dataset and the input RMS stability for a given average input energy. The correction factors are displayed as error bars to indicate the additional uncertainty introduced by increased input energy variability.

spectra, and were chosen based on the manufacturer's quoted optical resolution of 1.8 nm. A gradual increase in spectral stability, evidenced by a reduction in the SDs as percentages of the mean count values, was observed by increasing the input energy [Fig. 6(a)].

This effect was found to be more pronounced if the RMS stabilities of the input pulse energies were taken into account, as shown in Fig. 6(b), where the stability dataset has been scaled according to the input RMS stabilities. For comparison with the spectral stability scaling with input energy, the scaling of the RMS stabilities of the energy contained within the supercontinuum with increasing input energy (Fig. 7) was also analyzed.

The energy stability is approximately constant across the range of energies considered, with some indication of a weak trend toward increased stability with increasing input energy. Similarly to the spectral stability behavior, the trend becomes more pronounced (steeper) after correcting for the variations in input RMS energy stabilities, but the uncertainties are relatively large compared to the differences between stability values. The scaled RMS supercontinuum energy stabilities range between ~2.4% and ~4.5% for input energy RMS stabilities ranging between ~1.4% and 2%, so the K_2ZnCl_4 supercontinuum source has favorable energy stability properties considering its reliance on nonlinear optical spectral broadening processes.

Shape variations in the spectral stability plots (λ_i versus σ_{λ_i}) were observed as the driver pulse energies were increased, as shown in Fig. 8.

These manifested as both an overall decrease in the standard deviations in intensity counts measured in each bin, suggesting a global increase in spectral stability (reduction in unscaled σ_{glo} from 8.3% to 6.7%), and also apparent localized improvements in the stability of particular spectral regions, particularly around the edges of spectral peaks (400 nm, 970 nm). The effect is particularly pronounced close to 400 nm, the furthest generated wavelength from the drive wavelength, where σ_{λ_i}

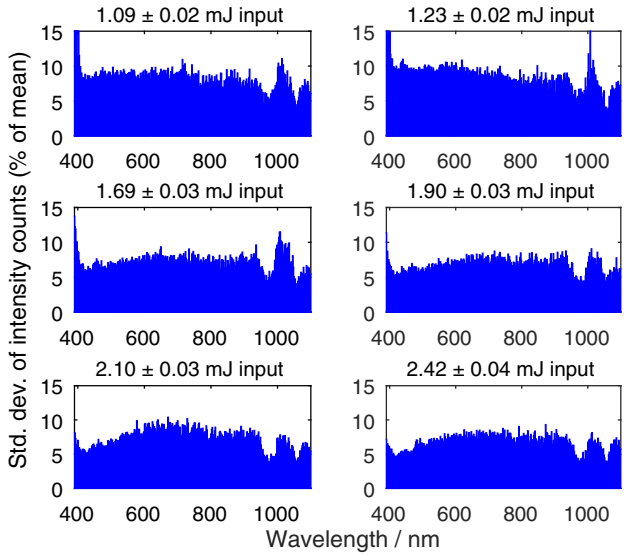


Fig. 8. Sample of spectral stability plots depicting σ_{λ_i}, the SD of the measured intensity counts as a percentage of the mean value for each 1.8 nm wide wavelength bin. Each plot was obtained using spectra measured at the various indicated input driver pulse energies.

decreases from ∼15% to ∼5% This is likely because there is a larger numbers of photons in these wavelength bands as the supercontinuum is driven more strongly, progressively improving the signal-to-noise ratio, which has a much more pronounced effect in the regions with small photon counts. The spectral stability plots in Fig. 8 are meaningful only for wavelength bands in which there is clearly measurable signal; otherwise, standard deviations of the counts as a percentage of the mean value in each band for each measured spectrum can become very large, as they only reflect the standard deviations in the mean counts due to instrument noise. Away from the edges of spectral features, the detected counts are far beyond the instrument noise level (<40 counts), with signal counts exceeding the noise level by ×100–1000, such that the global increase in spectral stability percentages is less pronounced. Hence, for spectral content between 410 and 970 nm, the spectral fluctuation inherent to the nonlinear broadening mechanisms dominates the detector noise. In regions where there are strong water absorption features, such as >970 and <1050 nm, the standard deviations are locally higher, reflecting the lower signal-to-noise ratios in the presence of absorption.

3. SPECTRAL CORRELATIONS ANALYSIS

Spectral correlation maps provide insight into the relationships between intensities in different regions of the supercontinuum spectrum and can be used quantify its dynamical evolution [26,29,31,60]. The spectral correlation $\rho(\lambda_1,\lambda_2)$ between wavelengths λ_1 and λ_2 is defined as

$$\rho(\lambda_1,\lambda_2)=\frac{\langle I(\lambda_1)I(\lambda_2)\rangle-\langle I(\lambda_1)\rangle\langle I(\lambda_2)\rangle}{\sqrt{(\langle I^2(\lambda_1)\rangle-\langle I(\lambda_1)\rangle^2)(\langle I^2(\lambda_2)\rangle-\langle I(\lambda_2)\rangle^2)}}, \quad (4)$$

where quantities inside angle brackets are the ensemble averages across (in this case) the ≈50 spectra taken at each input drive pulse energy. The correlations vary as $-1<\rho\leq 1$, where $\rho=1$ is by definition observed along the line $\lambda_1=\lambda_2$. Positive correlations indicate that spectral intensities $I(\lambda_1)$ and $I(\lambda_2)$ increase or decrease together, whereas a negative correlation arises where a spectral intensity component increases at the expense of the other and *vice versa*. This is informative about the transfer of energy among different spectral regions, and thus the spectral broadening mechanisms involved in the laser–liquid interaction by association. For example, the presence of a positive correlation between the relative intensities of two adjacent spectral regions suggests that they are generated by the same or directly linked processes, as might be seen with sideband generation associated with SPM or SPM followed by optical wave breaking. Strong correlations between particular separated and localized regions only could indicate the significance of anti-Stokes stimulated Raman scattering processes.

A correlation map spanning the full spectrum of the supercontinuum ($\Delta\lambda>600$ nm) is shown in Fig. 9, with the region around the 1054 pump wavelength shown in greater detail in Fig. 10(a). Yellow indicates perfect positive correlations, while cyan denotes negative correlation. Areas where there are no correlations are shown in black, such as the region below 400 nm where there is no measured spectral content above the noise level, so no correlation would be expected with

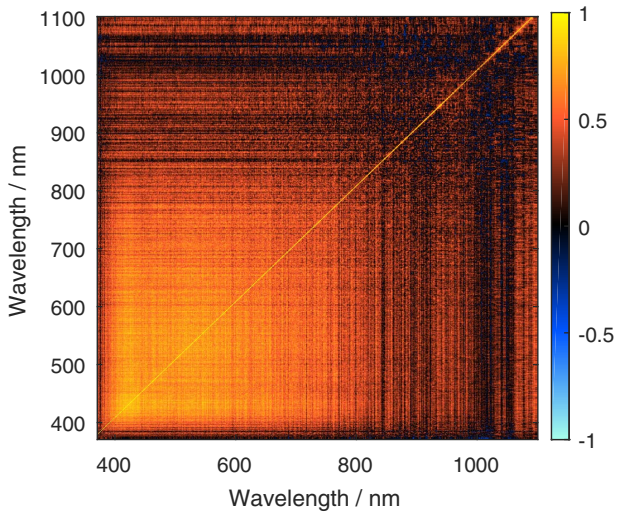


Fig. 9. Spectral correlation map covering the full measurable spectrum of the supercontinuum generated in the double-salt solution, measured for 1054 nm drive pulses of 2.42 ± 0.04 mJ energies and 500 ± 50 fs FWHM durations. The positively correlated (orange) region spanning 390–900 nm suggests that this part of the spectrum is generated via the same process, while the negative correlation between this wavelength band and the narrow region around the fundamental is consistent with sideband formation via self-phase modulation as energy is shifted from the drive pulse to the supercontinuum.

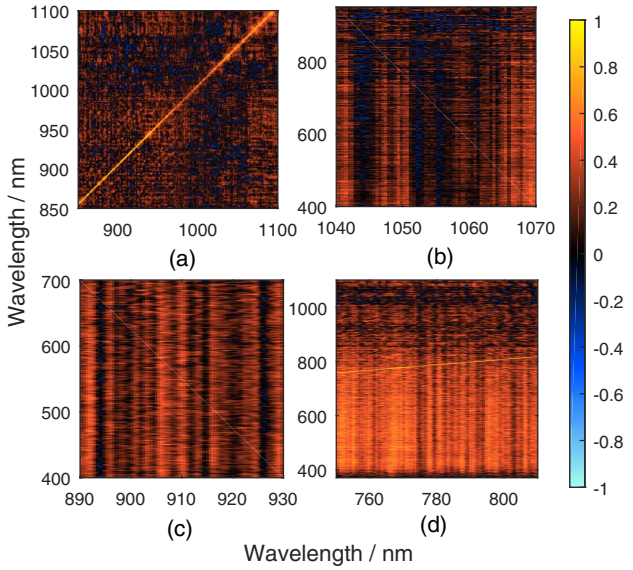


Fig. 10. Spectral correlation map covering multiple regions of the continuum in more detail. Input pulse energies of 2.42 ± 0.04 mJ were used. The region around the fundamental wavelength is shown in (a), with regions of negative correlation around the drive wavelength implying transfer of energy to the sidebands, visible in greater detail in (b). In (c), bands of negative correlation between the peaks at ∼894 and ∼927 nm and the rest of the supercontinuum imply that some secondary process shifts energy from these peaks into the visible spectral region. The effect of absorption features reducing the correlation magnitudes is examined in (d), where the map is centered on ∼780 nm, corresponding to the trough visible in Fig. 3.

the rest of the spectrum. The spectral correlation maps indicate that self-phase modulation within a dispersive medium (with initially unchirped pulses), possibly followed by additional coherent sideband generation via another mechanism such as optical wave breaking, are likely broadening mechanisms. We observe regions of strong positive correlation, far from the 1054 nm fundamental wavelength, across the 400–800 nm region (Fig. 9), whereas there are negative correlations between the residual component of the 3 nm FWHM bandwidth near-IR 1054 nm fundamental and the entire spectral region spanning 400–960 nm (correlation values of ≈ -0.5), which is not removed by the IR mirror in the beamline [Fig. 10(b)].

This suggests that energy is being shifted away from the fundamental into broad side bands, as would be expected from a mixture of nonlinear processes such as SPM and GVD followed by optical wave breaking. There are many nonlinear optical processes that could be responsible for spectral broadening, so it is likely that the observed spectra arise based on a complex interplay of multiple different nonlinear effects as well as some modulation contribution due to absorption in the liquid medium. It is, however, not possible to conclusively determine the dominant broadening mechanism within this work, as much of the spectral information is lost via absorption and the limited measurable spectral range, so any possible Stokes sidebands are not analyzable. The negatively correlated regions were observed to have weaker correlation values than the positively correlated areas, mainly due to the much lower signal levels in the fundamental spectral region, which consisted only of the leaked IR through a high-reflectivity IR mirror. The correlation maps are consistent with those reported by van de Walle *et al.* [31] arising from propagating short pulses through solid-core fibers or focusing them into bulk media, in their case YAG crystals. However, the supercontinuum was primarily in the mid-IR rather than the visible and near-IR, as is the case with the aqueous K_2ZnCl_4 solution.

Localized weak negative correlation bands between the spectral peaks at ~894 and ~927 nm and the full visible region [Fig. 10(c)] imply that there is some weak effect transferring energy between these features; this could be due to secondary self-phase modulation of light in these spectral regions, or alternatively another nonlinear effect resulting in spectral shifts. It is unlikely that this is an anti-Stokes Raman scattering effect, as the negative correlation is with the full band rather than a localized spectral region, which would be characteristic of photon energy gain from a particular water vibrational mode. In 24°C liquid-phase water, Raman modes are reported to be present at 3200 and 3400 cm^{-1} [61], corresponding to photon energy shifts of 0.397 and 0.422 eV, respectively. These would potentially result in shifts from 1054 nm to 789 and 776 nm, from 894 nm to 696 and 686 nm, and from 927 nm to 715 and 705 nm. A two-stage anti-Stokes Raman shift would result in peaks at approximately 630, 615, 583, 569, and 557 nm from the aforementioned initial peaks. While there are indeed slight negative correlations observed between the proposed fundamental wavelengths and the calculated Raman shifts, these do not stand out in terms of their correlation strengths from the large numbers of other wavelengths that are also negatively correlated with the fundamental wavelength and two main spectral peaks in the supercontinuum. Hence, we cannot conclude based on this evidence that Raman scattering contributes significantly toward the spectral broadening, in comparison to sideband-producing effects such as SPM followed by optical wave breaking, which are more consistent with the correlation maps.

The presence of water absorption features coinciding with certain areas of the spectral profile, as shown in Fig. 3, can also be examined using spectral correlations; regions containing strong absorption features relative to the strength of the spectral broadening processes should exhibit weaker correlations, as these dominate the spectral intensity content to a greater extent and lower the signal-to-noise ratios. In Fig. 10(d), around the spectral trough feature located at ~780 nm, some evidence of weaker correlations can be seen, along with a few bands where there is no correlation with the remainder of the spectrum. However, the effect is weak, as there is sufficient spectral content in this region to be well above the spectrometer's noise level, such that the dominant behavior for this region is still negative correlation with the region around the drive wavelength and positive correlation with the remainder of the supercontinuum generated by nonlinear effects producing distinct sidebands. The weakness of this effect further suggests that absorption modulation is only partly responsible for the spectral shapes observed.

4. CONCLUSIONS

We have demonstrated that the spectral and energy stability of a simple-to-implement and spatially smoothed supercontinuum laser source based on spectral broadening in a concentrated K_2ZnCl_4 double salt solution is limited to variation of only a few percent of the mean energy or spectral intensity values. This stability intrinsically depends on the energy stability of the infrared driver pulses, with white-light energy RMS stability values typically being approximately twice those of the driver pulses. Furthermore, a quadratic relationship between input and supercontinuum pulse energies was observed, while increasing the input energy has also been shown to improve the spectral stability and increase the efficiency of energy transfer from the IR into the supercontinuum. In addition, the use of a liquid nonlinear medium allows the source to be driven beyond its ionization threshold without causing permanent damage.

The shape of the supercontinuum spectrum appears to be determined partly by modulations due to absorption in the solvent (water), and an interplay between possibly several nonlinear processes, such as SPM followed by optical wave breaking. The source's stability, relatively high single-shot energy, and ~5 ps pulse durations (due to dispersive broadening in the liquid nonlinear medium) render it suitable for applications such as dynamic calibration of optical streak cameras in fast-sweep mode. The results represent a major improvement on previously published results concerning a supercontinuum source using K_2ZnCl_4 solutions [19], with an increase in spectral width of ~500 nm and supercontinuum energies of 40 μJ, approaching the preceding work's drive pulse energy of 80 μJ.

Analysis of the correlations between the intensities of different spectral peaks shows positive correlations, indicative of

sideband generation from a separate driver pulse that is characteristic of nonlinear effects such as SPM and GVD, leading to optical wave breaking. Furthermore, filaments were observed within the liquid, suggesting that the source operated in a regime of strong self-focusing. From these factors, we conclude that the spectral broadening is most likely driven by a complex mixture of nonlinear processes, such as SPM in a high n_2 and normally dispersive medium followed by further sideband generation via optical wave breaking, rather than soliton effects or stimulated Raman scattering.

Data underpinning this work can be found in Zenodo [62] and is made openly available under a CC-BY license.

Funding. Engineering and Physical Sciences Research Council (EPSRC) (1584149); Atomic Weapons Establishment (AWE) (30318116).

Acknowledgment. We would like to thank Dane Austin for advice related to supercontinuum generation and measurement.

REFERENCES

1. J. M. Dudley, G. Genty, and S. Coen, "Supercontinuum generation in photonic crystal fiber," Rev. Mod. Phys. **78**, 1135–1184 (2006).
2. B. Schenkel, J. Biegert, U. Keller, C. Vozzi, M. Nisoli, G. Sansone, S. Stagira, S. D. Silvestri, and O. Svelto, "Generation of 3.8-fs pulses from adaptive compression of a cascaded hollow fiber supercontinuum," Opt. Lett. **28**, 1987–1989 (2003).
3. M. A. Foster, A. L. Gaeta, Q. Cao, and R. Trebino, "Soliton-effect compression of supercontinuum to few-cycle durations in photonic nanowires," Opt. Express **13**, 6848–6855 (2005).
4. M. V. Tognetti and H. M. Crespo, "Sub-two-cycle soliton-effect pulse compression at 800 nm in photonic crystal fibers," J. Opt. Soc. Am. B **24**, 1410–1415 (2007).
5. A. Husakou and J. Herrmann, "Soliton-effect pulse compression in the single-cycle regime in broadband dielectric-coated metallic hollow waveguides," Opt. Express **17**, 17636–17644 (2009).
6. A. Labruyère, A. Tonello, V. Couderc, G. Huss, and P. Leproux, "Compact supercontinuum sources and their biomedical applications," Opt. Fiber Technol. **18**, 375–378 (2012).
7. N. Nishizawa, "Generation and application of high-quality supercontinuum sources," Opt. Fiber Technol. **18**, 394–402 (2012).
8. J. Lee, "Broadband, high power, erbium fibre ASE-based CW supercontinuum source for spectrum-sliced WDM PON applications," Electron. Lett. **42**, 549–550 (2006).
9. C. Kaminski, R. Watt, A. Elder, J. Frank, and J. Hult, "Supercontinuum radiation for applications in chemical sensing and microscopy," Appl. Phys. B **92**, 367–378 (2008).
10. J. Kasparian, M. Rodriguez, G. Méjean, J. Yu, E. Salmon, H. Wille, R. Bourayou, S. Frey, Y.-B. André, A. Mysyrowicz, R. Sauerbrey, J.-P. Wolf, and L. Wöste, "White-light filaments for atmospheric analysis," Science **301**, 61–64 (2003).
11. F. Silva, D. R. Austin, A. Thai, M. Baudisch, M. Hemmer, D. Faccio, A. Couairon, and J. Biegert, "Multi-octave supercontinuum generation from mid-infrared filamentation in a bulk crystal," Nat. Commun. **3**, 807 (2012).
12. J. C. Knight, T. A. Birks, D. M. Atkin, and P. St. J. Russell, "Pure silica single-mode fibre with hexagonal photonic crystal cladding," in *Optical Fiber Communication Conference* (Optical Society of America, 1996), paper PD3.
13. P. St. J. Russell, "Photonic crystal fibers," Science **299**, 358–362 (2003).
14. P. St. J. Russell, "Photonic-crystal fibers," J. Lightwave Technol. **24**, 4729–4749 (2006).
15. N. Y. Joly, J. Nold, W. Chang, P. Hölzer, A. Nazarkin, G. K. L. Wong, F. Biancalana, and P. St. J. Russell, "Bright spatially coherent wavelength-tunable deep-UV laser source using an Ar-filled photonic crystal fiber," Phys. Rev. Lett. **106**, 203901 (2011).
16. F. Belli, A. Abdolvand, W. Chang, J. C. Travers, and P. St. J. Russell, "Vacuum-ultraviolet to infrared supercontinuum in hydrogen-filled photonic crystal fiber," Optica **2**, 292–300 (2015).
17. J. Bethge, A. Husakou, F. Mitschke, F. Noack, U. Griebner, G. Steinmeyer, and J. Herrmann, "Two-octave supercontinuum generation in a water-filled photonic crystal fiber," Opt. Express **18**, 6230–6240 (2010).
18. M. Chemnitz, M. Gebhardt, C. Gaida, F. Stutzki, J. Kobelke, J. Limpert, A. Tünnermann, and M. A. Schmidt, "Hybrid soliton dynamics in liquid-core fibres," Nat. Commun. **8**, 42 (2017).
19. T. Jimbo, V. L. Caplan, Q. X. Li, Q. Z. Wang, P. P. Ho, and R. R. Alfano, "Enhancement of ultrafast supercontinuum generation in water by the addition of Zn^{2+} and K^{+} cations," Opt. Lett. **12**, 477–479 (1987).
20. J. Y. Zhou, H. Z. Wang, and Z. X. Yu, "Efficient generation of ultrafast broadband radiation in a submillimeter liquid-core waveguide," Appl. Phys. Lett. **57**, 643–644 (1990).
21. P. Vasa, J. A. Dharmadhikari, A. K. Dharmadhikari, R. Sharma, M. Singh, and D. Mathur, "Supercontinuum generation in water by intense, femtosecond laser pulses under anomalous chromatic dispersion," Phys. Rev. A **89**, 043834 (2014).
22. A. N. Tcypkin, S. E. Putilin, M. V. Melnik, E. A. Makarov, V. G. Bespalov, and S. A. Kozlov, "Generation of high-intensity spectral supercontinuum of more than two octaves in a water jet," Appl. Opt. **55**, 8390–8394 (2016).
23. J. A. Dharmadhikari, G. Steinmeyer, G. Gopakumar, D. Mathur, and A. K. Dharmadhikari, "Femtosecond supercontinuum generation in water in the vicinity of absorption bands," Opt. Lett. **41**, 3475–3478 (2016).
24. H. Li, Z. Shi, X. Wang, L. Sui, S. Li, and M. Jin, "Influence of dopants on supercontinuum generation during the femtosecond laser filamentation in water," Chem. Phys. Lett. **681**, 86–89 (2017).
25. D. Solli, G. Herink, B. Jalali, and C. Ropers, "Fluctuations and correlations in modulation instability," Nat. Photonics **6**, 463–468 (2012).
26. B. Wetzel, A. Stefani, L. Larger, P. A. Lacourt, J. M. Merolla, T. Sylvestre, A. Kudlinski, A. Mussot, G. Genty, F. Dias, and J. M. Dudley, "Real-time full bandwidth measurement of spectral noise in supercontinuum generation," Sci. Rep. **2**, 882 (2012).
27. Z. Ren, Y. Xu, Y. Qiu, K. K. Y. Wong, and K. Tsia, "Spectrally-resolved statistical characterization of seeded supercontinuum suppression using optical time-stretch," Opt. Express **22**, 11849–11860 (2014).
28. H. Saghaei, M. K. Moravvej-Farshi, M. Ebnali-Heidari, and M. N. Moghadasi, "Ultra-wide mid-infrared supercontinuum generation in As40Se60 chalcogenide fibers: solid core PCF versus SIF," IEEE J. Sel. Top. Quantum Electron. **22**, 279–286 (2016).
29. X. Wang, D. Bigourd, A. Kudlinski, K. K. Y. Wong, M. Douay, L. Bigot, A. Lerouge, Y. Quiquempois, and A. Mussot, "Correlation between multiple modulation instability side lobes in dispersion oscillating fiber," Opt. Lett. **39**, 1881–1884 (2014).
30. Q. Cao, X. Gu, E. Zeek, M. Kimmel, R. Trebino, J. Dudley, and R. S. Windeler, "Measurement of the intensity and phase of supercontinuum from an 8-mm-long microstructure fiber," Appl. Phys. B **77**, 239–244 (2003).
31. A. van de Walle, M. Hanna, F. Guichard, Y. Zaouter, A. Thai, N. Forget, and P. Georges, "Spectral and spatial full-bandwidth correlation analysis of bulk-generated supercontinuum in the mid-infrared," Opt. Lett. **40**, 673–676 (2015).
32. T. M. Fortier, J. Ye, S. T. Cundiff, and R. S. Windeler, "Nonlinear phase noise generated in air-silica microstructure fiber and its effect on carrier-envelope phase," Opt. Lett. **27**, 445–447 (2002).
33. K. L. Corwin, N. R. Newbury, J. M. Dudley, S. Coen, S. A. Diddams, K. Weber, and R. S. Windeler, "Fundamental noise limitations to supercontinuum generation in microstructure fiber," Phys. Rev. Lett. **90**, 113904 (2003).
34. D. R. Solli, C. Ropers, and B. Jalali, "Active control of rogue waves for stimulated supercontinuum generation," Phys. Rev. Lett. **101**, 233902 (2008).

35. W. J. Tomlinson, R. H. Stolen, and A. M. Johnson, "Optical wave breaking of pulses in nonlinear optical fibers," Opt. Lett. **10**, 457–459 (1985).
36. A. M. Heidt, J. S. Feehan, J. H. V. Price, and T. Feurer, "Limits of coherent supercontinuum generation in normal dispersion fibers," J. Opt. Soc. Am. B **34**, 764–775 (2017).
37. J. D. Harvey, R. Leonhardt, S. Coen, G. K. L. Wong, J. Knight, W. J. Wadsworth, and P. St. J. Russell, "Scalar modulation instability in the normal dispersion regime by use of a photonic crystal fiber," Opt. Lett. **28**, 2225–2227 (2003).
38. A. Demircan and U. Bandelow, "Supercontinuum generation by the modulation instability," Opt. Commun. **244**, 181–185 (2005).
39. R. L. Carman, R. Y. Chiao, and P. L. Kelley, "Observation of degenerate stimulated four-photon interaction and four-wave parametric amplification," Phys. Rev. Lett. **17**, 1281–1283 (1966).
40. R. Stolen, "Phase-matched-stimulated four-photon mixing in silica-fiber waveguides," IEEE J. Quantum Electron. **11**, 100–103 (1975).
41. D. Nodop, C. Jauregui, D. Schimpf, J. Limpert, and A. Tünnermann, "Efficient high-power generation of visible and mid-infrared light by degenerate four-wave-mixing in a large-mode-area photonic-crystal fiber," Opt. Lett. **34**, 3499–3501 (2009).
42. F. M. Mitschke and L. F. Mollenauer, "Discovery of the soliton self-frequency shift," Opt. Lett. **11**, 659–661 (1986).
43. J. P. Gordon, "Theory of the soliton self-frequency shift," Opt. Lett. **11**, 662–664 (1986).
44. X. Liu, C. Xu, W. H. Knox, J. K. Chandalia, B. J. Eggleton, S. G. Kosinski, and R. S. Windeler, "Soliton self-frequency shift in a short tapered air-silica microstructure fiber," Opt. Lett. **26**, 358–360 (2001).
45. K. S. Abedin and F. Kubota, "Widely tunable femtosecond soliton pulse generation at a 10-GHz repetition rate by use of the soliton self-frequency shift in photonic crystal fiber," Opt. Lett. **28**, 1760–1762 (2003).
46. E. R. Andresen, V. Birkedal, J. Thøgersen, and S. R. Keiding, "Tunable light source for coherent anti-Stokes Raman scattering microspectroscopy based on the soliton self-frequency shift," Opt. Lett. **31**, 1328–1330 (2006).
47. J. H. Lee, J. van Howe, C. Xu, and X. Liu, "Soliton self-frequency shift: experimental demonstrations and applications," IEEE J. Sel. Top. Quantum Electron. **14**, 713–723 (2008).
48. A. A. Voronin and A. M. Zheltikov, "Soliton self-frequency shift decelerated by self-steepening," Opt. Lett. **33**, 1723–1725 (2008).
49. B. Stoicheff, "Characteristics of stimulated Raman radiation generated by coherent light," Phys. Lett. **7**, 186–188 (1963).
50. N. Bloembergen and P. Lallemand, "Complex intensity-dependent index of refraction, frequency broadening of stimulated Raman lines, and stimulated Rayleigh scattering," Phys. Rev. Lett. **16**, 81–84 (1966).
51. T. K. Gustafson, J. P. Taran, H. A. Haus, J. R. Lifsitz, and P. L. Kelley, "Self-modulation, self-steepening, and spectral development of light in small-scale trapped filaments," Phys. Rev. **177**, 306–313 (1969).
52. A. Talebpour, A. Bandrauk, J. Yang, and S. Chin, "Multiphoton ionization of inner-valence electrons and fragmentation of ethylene in an intense Ti:sapphire laser pulse," Chem. Phys. Lett. **313**, 789–794 (1999).
53. X. Li, L. H. Liu, J. Zhao, and J. Tan, "Optical properties of sodium chloride solution within the spectral range from 300 to 2500 nm at room temperature," Appl. Spectrosc. **69**, 635–640 (2015).
54. D. X. Hammer, R. J. Thomas, G. D. Noojin, B. A. Rockwell, P. K. Kennedy, and W. P. Roach, "Experimental investigation of ultrashort pulse laser-induced breakdown thresholds in aqueous media," IEEE J. Quantum Electron. **32**, 670–678 (1996).
55. S. Patankar, E. T. Gumbrell, T. S. Robinson, H. F. Lowe, S. Giltrap, C. J. Price, N. H. Stuart, P. Kemshall, J. Fyrth, J. Luis, J. W. Skidmore, and R. A. Smith, "Multiwavelength interferometry system for the Orion laser facility," Appl. Opt. **54**, 10592–10598 (2015).
56. S. Patankar, E. T. Gumbrell, T. S. Robinson, E. Floyd, N. H. Stuart, A. S. Moore, J. W. Skidmore, and R. A. Smith, "Absolute calibration of optical streak cameras on picosecond time scales using supercontinuum generation," Appl. Opt. **56**, 6982–6987 (2017).
57. G. M. Hale and M. R. Querry, "Optical constants of water in the 200-nm to 200-μm wavelength region," Appl. Opt. **12**, 555–563 (1973).
58. A. Braun, G. Korn, X. Liu, D. Du, J. Squier, and G. Mourou, "Self-channeling of high-peak-power femtosecond laser pulses in air," Opt. Lett. **20**, 73–75 (1995).
59. S. Rostami, M. Chini, K. Lim, J. P. Palastro, M. Durand, J.-C. Diels, L. Arissian, M. Baudelet, and M. Richardson, "Dramatic enhancement of supercontinuum generation in elliptically-polarized laser filaments," Sci. Rep. **6**, 20363 (2016).
60. P. Béjot, J. Kasparian, E. Salmon, R. Ackermann, and J.-P. Wolf, "Spectral correlation and noise reduction in laser filaments," Appl. Phys. B **87**, 1–4 (2007).
61. D. M. Carey and G. M. Korenowski, "Measurement of the Raman spectrum of liquid water," J. Chem. Phys. **108**, 2669–2675 (1998).
62. T. S. Robinson, "Spectral characterization of a supercontinuum source based on nonlinear broadening in an aqueous K_2ZnCl_4 salt solution," Zenodo (2017), https://zenodo.org/record/883028.

155.198.12.147 {ts '2018-01-05 11:22:29'}